Published in final edited form as:
Biochemistry. 2013 April 30; 52(17): 2933–2948. doi:10.1021/bi400180d.

Comparative Proteomic Analysis Identifies Age-Dependent Increases in the Abundance of Specific Proteins after Deletion of the Small Heat Shock Proteins αA- and αB-Crystallin

Usha P. Andley[1,*], **James P. Malone**[2], **Paul D. Hamilton**[3], **Nathan Ravi**[1,3], and **R. Reid Townsend**[2]

[1]Department of Ophthalmology and Visual Sciences, Washington University School of Medicine, St. Louis, Missouri, U.S.A

[2]Department of Medicine, Washington University School of Medicine, St. Louis, Missouri, U.S.A

[3]Department of Research, Veterans Administration Hospital, St. Louis, Missouri, U.S.A

Abstract

Mice with deletion of genes for small heat shock proteins αA- and αB-crystallin (αA/αB$^{-/-}$) develop cataracts. We used proteomic analysis to identify lens proteins that change in abundance after deletion of these α-crystallin genes. Wild-type (WT) and αA/αB$^{-/-}$ knockout (DKO) mice were compared using two-dimensional difference gel electrophoresis and mass spectrometric analysis, and protein identifications were validated by Mascot proteomic software. The abundance of histones H2A, H4, and H2B fragment, and a low molecular weight β1-catenin increased 2- to 3-fold in postnatal day 2 lenses of DKO lenses compared with WT lenses. Additional major increases were observed in abundance of βB2-crystallin and vimentin in 30-day-old lenses of DKO animals compared with WT animals. Lenses of DKO mice were comprised of 9 protein spots containing βB2-crystallin at 10- to 40-fold higher abundance and 3 protein spots containing vimentin at ≥ 2-fold higher abundance than in WT lenses. Gel permeation chromatography identified a unique 328 kDa protein in DKO lenses, containing β-crystallin, demonstrating aggregation of β-crystallin in the absence of α-crystallins. Together, these changes provide biochemical evidence for possible functions of specific cell adhesion proteins, cytoskeletal proteins, and crystallins in lens opacities caused by the absence of the major chaperones, αA- and αB-crystallins.

Keywords

Crystallin; knockout; proteomics; substrate; alpha-crystallin; chaperone

The mammalian lens expresses high levels of α-, β-, and γ-crystallins to maintain a smooth refractive index (RI) gradient, which is essential for lens transparency (1). Expression of crystallins begins at an early developmental age (2). They are synthesized throughout life but do not turnover, and are distributed at high levels in terminally differentiated lens fiber cells (3). α-crystallins, which constitute approximately 50% of the human lens at birth, play an important role in lens transparency by binding to partially denatured proteins and

[*]Corresponding author: Usha P. Andley, Department of Ophthalmology and Visual Sciences, Washington University School of Medicine, 660 S. Euclid Avenue, Campus Box 8096, St. Louis, Missouri 63110, U.S.A. 314-362-7167 (Tel), 314-362-3638 (Fax), andley@vision.wustl.edu.

SUPPORTING INFORMATION

Additional supplemental figures and tables are available free of charge via the Internet at http://pubs.acs.org.

preventing their denaturation during the normal course of lens aging (4). The α-crystallins are molecular chaperones of the small heat shock protein family, and prevent the nonspecific aggregation of denaturing proteins (5). They are also phosphoproteins with autokinase activity (6). Mice with targeted gene deletion of one or both of the α-crystallin genes have been generated to elucidate the in vivo function of these proteins (7, 8). This knockout results in mice with opacities (cataracts), a smaller lens, and lens epithelial cells exhibiting increased cell death (7, 9, 10). Targeted knockout of αB-crystallin in mice does not result in cataracts but causes an increased tendency of lens epithelial cells to hyperproliferate in culture (8, 11, 12). Deletion of both αA- and αB-crystallin genes in double knockout (DKO) mice results in animals that develop cataracts at birth and exhibit increased expression of caspases in the lens, resulting in enhanced apoptosis and smaller lenses (13). Lens epithelial cells derived from DKO mice have slower cell cycle kinetics (14), and the microtubule-associated protein tau is upregulated in lens fiber cells (15).

Whether loss of α-crystallin chaperone activity in the lens causes a change in the abundance of other proteins has not been investigated. Although the chaperone activity of the α-crystallins is critical for maintaining lens transparency, information about the in vivo substrates of these chaperones is limited. The α-crystallins are lens cytoplasmic proteins, but they also associate with lens membranes, where they regulate cell signaling (16). In addition, α-crystallins are important for maintaining tubulin in a folded conformation which is necessary for its assembly into microtubules (17). These changes are thought to be caused in part by tubulin protein denaturation, and suggest that tubulin is an important target of the chaperone function of α-crystallins (12, 17). αB-crystallin associates with other cytoskeletal proteins such as vimentin and actin, and prevents inappropriate aggregation of the cytoskeletal polymers (18, 19). Both α-crystallins also bind to destabilized βB1-crystallin (20).

Although many cellular functions have been linked with α-crystallins, a detailed analysis of alterations in protein abundance in lenses of (DKO) mice has not been performed. Analysis of proteins that are up- or downregulated in these lenses has the potential to identify in vivo substrates for the chaperone activity of the α-crystallins. This analysis may also provide greater insight into the mechanism of cataract formation in the absence of α-crystallins in the lens. Because α-crystallins decrease with age in human lenses and aggregate to form high molecular weight, water-insoluble species with aging and cataract, such an understanding may help in the development of effective strategies for both treatment and prevention of cataracts.

In the present study, we analyzed the abundance of proteins in DKO mice lenses by proteomics, mass spectrometry, immunoblotting, and gel permeation chromatography (GPC). Our proteomic analysis suggests that β1-catenin forms a low molecular weight degradation product, and the amount of histones is enhanced in lenses of postnatal DKO mice. Our results also demonstrate that vimentin is cross-linked and associated with tubulin in young DKO lenses, suggesting that these proteins are modulated by the expression of α-crystallins in vivo. To better understand the implications for lens remodeling induced by absence of α- crystallins, we also used Ingenuity Pathway Analysis (IPA) to identify the placement of α-crystallins within a putative biological context.

Materials and Methods

Animals and lenses

All mouse procedures were approved by the Washington University animal use committee. The wild-type (WT) mouse strain was the 129SvJ mouse. DKO mice were obtained from Dr. Eric Wawrousek (National Eye Institute, Bethesda, MD). They were generated by

interbreeding αAKO-127 knockout mice with αBKO-168 mice (13). The AKO-127 knockout mice were generated by targeted disruption of the αA-crystallin gene (7), and the αBKO-168 knockout mice were generated by targeted disruption of the αB-crystallin gene (8). The knockout vector eliminated the common promoter region of the αB-crystallin and HSPB2 genes as well as almost all of the coding regions of these two genes (8). However, HSPB2 was not expressed in the lens, and its deletion was not expected to yield any lens phenotypes.

Preparation of samples for mass spectrometry and two-dimensional difference gel electrophoresis (2D-DIGE)

Lenses of two different age groups were analyzed by mass spectrometry. Group 1 lenses were from 2-day-old mice (2–4 mice in each replicate set of WT1, WT2, and DKO1; and WT3, WT4, and DKO2). Whole lenses were analyzed in the first group, and the data are presented in Figures 1, 2, S1, S2, and Table 1. Group 2 lenses were collected from three sets of older mice: WT5, 67-day-old (3 mice) and 76-day-old (5 mice). These are referred to as 70-day-old mice for ease of reading, plus WT6 was comprised of 35-day-old (8 mice) and DKO3 was comprised of 30-day-old (8 mice). In addition to comparison of age-matched WT6 and DKO3 mice, WT lenses of two different ages, 35-day-old and 67- to 76-day-old, were also compared in the same experiment. In Group 2, lenses were dissected into epithelial and cortical fiber cell fractions because of the high concentration of crystallins present in this age group. For this experiment, we combined epithelial fractions from 16 WT lenses and 16 DKO lenses. Proteomic analyses results for Group 2 are presented in Figures 3, S3, and Tables 2, 3. Additional experiments with WT and DKO lenses showed similar 2D-DIGE results and were not analyzed further.

For 2D-DIGE, lens tissue was placed in lysis buffer [30 mM Tris-HCl, pH 8.5, 2 M thiourea, 7 M urea, 4% CHAPS, 1× complete protease inhibitor cocktail tablets (Roche, Indianapolis, IN)], then homogenized, and centrifuged to remove insoluble proteins. Lens proteins (50 μg) were labeled with 400 pmol of Cy2, Cy3, or Cy5. 2D-DIGE was performed at the Proteomics Core Laboratory at the Washington University School of Medicine according to published methods (21).

Analysis of proteomic data and database searching

Single gel analysis was performed to compare WT and DKO lenses (shown in Tables 1–3). All tandem mass spectrometry samples were analyzed using Mascot (Matrix Science, London, UK; version 2.1.1.0) as previously described (21). Mascot was set to search the Uniprot mouse database (downloaded 12/28/2010, 135387 entries), using trypsin as the digestion enzyme, with a fragment ion mass tolerance of 0.80 Da and a parent ion tolerance of 50.0 PPM from the LTQ FT. The QSTAR data was searched using parent and fragment tolerance of 0.1 Da. The iodoacetamide derivative of cysteine was specified in Mascot as a fixed modification and methionine as a variable modification (21). Scaffold software (v. 3.6.1) was used to display proteomic data.

Knowledge-based network analysis

Ingenuity Pathways software was used for the analysis of networks based on the proteomics data shown in Tables 1–3 as described previously (22).

Immunoblotting

Lenses were homogenized on ice in 400 or 500 μl of phosphate-buffered saline (PBS) containing protease inhibitors as described previously (23). Homogenates were centrifuged at 10,000 × *g* at 4°C, and the resulting supernatants were collected (water-soluble fraction).

Pellets were resuspended in 125 μl of 8 M urea in PBS containing protease inhibitor, incubated at room temperature for 10 min, and centrifuged at 4°C. The supernatant was then collected (water-insoluble fraction). Protein concentrations were determined using the Bio-Rad Protein Assay. All samples were supplemented with sample buffer (4×) and reducing agent (10×; Invitrogen). Soluble fraction samples were heated at 95°C for 5 min. Equal amounts of total protein (15–40 μg) were then separated on 10% or 4–12% precast NuPAGE gels (Invitrogen). Soluble and insoluble fractions were analyzed on the same gel. For immunoblot analysis, proteins were transferred to a polyvinylidene fluoride membrane and probed with antibodies specific for βB2-crystallin (Enzo Life Sciences) and vimentin (provided by Paul FitzGerald, Davis, CA).

Analytical chromatography and data analysis

High-performance liquid chromatography-GPC was performed using a VE 1122 pump with a VE 7510 degasser (Viscotek/Malvern) equipped with a TDA302 triple detector system that measured refractive index (RI), multi-angle laser light scattering, and viscosity, as described previously (24, 25). The latter was supplemented with a model 2501 UV detector set at 280 nm. Two columns were connected in series: a Poly (Analytic) PAP-402.5 (Lausanne, Switzerland) and a G4000PWXL (Tosoh Biosep). Viscotek Omnisec software was used to calculate the RI area, weight-averaged molecular weight, intrinsic viscosity, and hydrodynamic radius (R_h). Lens proteins from postnatal and adult mice were analyzed using this column system. Samples were injected in a volume of 100–300 μl. The flow rate was 0.8 ml/min, and the column buffer contained modified Dulbecco's PBS without $CaCl_2$ and $MgCl_2$ (Sigma-Aldrich). Fractions from the column were then collected for immunoblot analysis. Initially, the amount of protein present in the WT and DKO mutant lens water-soluble fractions was calculated using the RI area from the initial run. Samples of each condition were then rerun using approximately equal amounts of total protein. The concentration of protein applied to the column was 1 mg/ml. Column fractions of each condition were collected at 1-min intervals (800 μl/tube). Four lenses were analyzed per age and genotype. Chromatography runs were repeated three times.

Quantitative reverse transcriptase-polymerase chain reaction (RT-PCR)

Total RNA from WT and DKO mouse lenses was isolated using a Qiagen kit. One μg of total RNA was used for each sample to prepare cDNA. RNA was treated with DNase, and first-strand cDNA synthesis was performed using a kit from Invitrogen and Oligo(dT) as a primer. Primers were synthesized by Integrated DNA Technologies (Coralville, IA), and their concentrations were optimized using the manufacturer's recommendations. To optimize the primers, RT-PCR was performed, and products were resolved on 1.5% agarose gels to ascertain that a single band of the correct size was obtained. Real time-PCR was performed using a supermix containing the fluorescent dye SYBR Green (BioRad) as described previously (15, 26). The increase in fluorescence was detected using the iCycler (BioRad). The relative quantification of gene expression was performed using the standard curve method according to the manufacturer's instructions (BioRad). For comparisons between WT and DKO samples, a standard curve of cycle thresholds for several serial dilutions of an RNA sample was established and then used to calculate the relative abundance levels of mRNA. The expression levels of βB2-crystallin and vimentin mRNAs were determined relative to that for glyceraldehyde 3-phosphate dehydrogenase (GAPDH) in the same sample. All RT-PCR reactions were performed in triplicate, and two independent experiments were performed.

Results

Increased abundance of β1-catenin fragments and histones in lenses of 2-day-old DKO mice

To examine whether the amount of other proteins changed in the DKO lenses, we performed a 2D-DIGE comparison of two WT samples (WT1 and WT2 labeled with Cy3 and Cy5, respectively) and one DKO (DKO1) lens sample labeled with Cy2 on a single gel. There were clear differences between protein levels of several spots in WT vs. DKO lenses (Figure 1 and S1). The differentially expressed spots on the gel were picked and further analyzed by mass spectrometry. Table 1 compares the proteins present in 2-day-old WT and DKO lenses. Three-dimensional data sets for some of the protein spots that showed significant changes are shown in Figure 2, and sequence coverage for these spots is shown in Figure S2. The abundance of β1-catenin and histones H2A, H4, and H2B (fragment) increased in DKO lenses. The molecular weight of these β1-catenin-containing spots was ~15 kDa, suggesting that β1-catenin in DKO lenses is degraded or cleaved from the intact 85 kDa molecule. An additional set of WT and DKO samples was analyzed by 2D-DIGE to demonstrate that the observed changes were not an artifact of the Cy dye labels. The WT samples were labeled with Cy2 and Cy3 and the DKO sample was labeled with Cy5 to confirm the proteomic changes. These results are shown in the last five rows of Table 1, and confirm the increase in amount of β1-catenin. Altogether, 9 protein spots containing β1-catenin (spots 6171, 6278, 6308, 6463, 6502, 6696, 7235, 1093, and 6908; Table 1) increased in the DKO1 lenses. In addition, spot 3027 containing βB1-crystallin (molecular weight 40–50 kDa) increased nearly 5-fold in DKO lenses, whereas spot 4946 containing βB1-crystallin (molecular weight 20–30 kDa) decreased nearly 3-fold. These results suggest that βB1-crystallin became cross-linked to form a dimer in the absence of α-crystallin.

Increased abundance of βB2-crystallin and vimentin in lens epithelial fractions of 30- to 70-day-old DKO mice

In Figure 3, we compare the proteins of 70-day-old WT (WT5) with 35-day-old WT (WT6) mice, and 35-day-old WT (WT6) mice with 30-day-old DKO (DKO3) lens epithelial fractions. Mass spectrometry-based proteomic analyses of these proteins are presented in Table 2.

To compare age-matched WT and DKO lenses, we first identified proteins of epithelial fractions from 30-day-old lenses that changed in amount after deletion of αA- and αB-crystallins. Protein spots that changed more than 1.5-fold in amount in this comparison were considered significant ($p < 0.05$). Fold changes in these proteins are listed in the last column of Table 2 (WT6 vs. DKO3). Proteins that increased in amount in DKO lenses are represented by the red spots in Figure 3A. Figures 3B and 3C show the differentially expressed spots on this gel that were picked and further analyzed. The analysis identified changes in the abundance of βB2-crystallin and vimentin in DKO lenses, and 3D data sets for some protein spots are shown in Figure 4. Figure S3 shows the sequence coverage for βB2-crystallin and vimentin, respectively, in WT5, WT6, and DKO3 lenses. Similarly, lens cortical fiber cell proteins also exhibited an increase in abundance of βB2-crystallin at the same position on the gel. However, because of the greater overall amount of crystallins in the cortical fiber cells of the 30-day-old lenses than in epithelial cells, these lens cortical fiber gels were not analyzed further.

The abundance of protein spot 2799 (vimentin and α-tubulin) was 2.39-fold higher in DKO3 lenses than in WT6 lenses (Table 2). The abundances of more basic forms of vimentin (spot 3259) decreased in DKO3 lenses. Spot 3259 also had a lower molecular weight than other vimentin-containing protein spots, including spots 2799 and 3080. In contrast, the

abundance of spot 2787 increased approximately 3-fold in DKO3 lenses, but this spot was more basic than 3259. These proteins are listed in Table 2.

Among the spots containing βB2-crystallin, spot 4418 exhibited a 49-fold increase in abundance in DKO3 lenses compared with its amount in WT6 lenses (shown in the last column of Table 2). Other spots that contained only βB2-crystallin, including spots 4430, 4431, 4446, 4491, and 4636, increased in abundance in DKO3 lenses compared with their amounts in WT5 or WT6 lenses. Additionally, the abundances of spots 4421 (βB1, βB3, and other proteins) and 4443 (βB1 and βB2-crystallin) was 42-fold higher in DKO3 lenses than in WT6 lenses. Interestingly, spot 4446 (βB2-crystallin only) was much more basic than the other βB2-crystallin spots, and its abundance increased 5.8-fold in DKO3 lenses compared with that in WT6 lenses. In contrast, the abundance of spot 4457 (βB3, βB2, and αB-crystallin) decreased 1.6-fold in DKO3 lenses compared to that in WT6 lenses, and also became more acidic. These observations suggest that in DKO lenses there was a loss of more acidic forms and an increase in more basic forms of βB2-crystallin.

In addition to βB2-crystallin and vimentin, changes in DKO3 lenses included an approximately 4-fold increase in the abundance of proteasome activator complex subunit 2 (spot 4115). In addition, spot 4224 exhibited a 2.5-fold increase in abundance, and it also became more basic in DKO3 lenses than WT6 lenses. This is in contrast to spot 5247 containing ubiquitin-like protein ISG15, which exhibited a 4.3-fold higher abundance in DKO3 lenses than in WT6 lenses, plus had a lower molecular weight and a more basic pI than spot 4224 (Table 2 and Figure 3).

We next compared the abundances of proteins in the epithelial fractions from 35-day-old and 70-day-old wild-type lenses, which revealed significant age-related changes in the expression of proteins (Table 2, column 6). For example, the abundances of cross-linked vimentin and tubulin (spot 2799), and αA- and βB2-crystallin (spot 3259) were lower in 35-day-old lenses than in 70-day-old lenses. This cross-linking would be expected to occur at a higher level in 70-day-old lenses. Similarly, the abundances of βB2-crystallin (spots 4425 and 4443) and βB3-crystallin (spot 4457) were 2- to 3-fold lower in 35-day-old lenses than in 70-day-old lenses. These β-crystallin spots may be additional and/or modified forms of these proteins, as changes in β-crystallin expression and increases in protein modification have been reported with age during the first 6 weeks of mouse lens growth (27).

Spot 4474 was one of three abundant protein spots whose abundance decreased 12-fold in DKO3 lenses compared to that in WT6 lenses. Spot 4644, another major spot in WT6 lenses that decreased in abundance in DKO3 lenses decreased 21-fold in DKO3 lenses compared with WT6 lenses. Similarly, the abundance of spot 4871, the last major spot identified as αA-crystallin only, decreased 22-fold in DKO3 lenses compared to that WT6 lenses. Another spot that decreased substantially in abundance and contained α-crystallin peptides was spot 4778 (αA- and αB-crystallins), the abundance of which decreased 13-fold in DKO3 lenses compared to WT6 lenses. These data confirm the depletion of αA-crystallin and αB-crystallin in the DKO lens.

To obtain a general perspective of cellular systems affected in the DKO lens, we analyzed the proteins identified by mass spectrometric analysis in all of the experiments (Tables 1–3) by mapping them to existing networks. Ingenuity Pathways software analysis generated seven different networks, four of which are shown in Figure 5, with additional networks shown in Figure S3. One network generated by this approach included STMN, which interacts with SOD1 (Figure 5A). SOD1 acts upon αB-crystallin and the GST kinases GSTP1 and GSTM1. A second network (Figure 5B) included chaperones (HSP, CCT4, and Hsp90), DNA topoisomerase TOPB1, the 26S proteasome, as well as the cytoskeletal

proteins tubulin, actin, and vimentin, which have been shown to interact with αA- and αB-crystallin. A third network (Figure 5C) highlighted CTNNB1 binding with SMARCA4, a member of the SW1/SNF family of proteins with ATPase and helicase activities that affect lens development and cataract (28, 29). CTNNB1 is also involved with interactions and regulatory functions of the signaling proteins Ras, TGFβ, ERK, and Akt, and regulates Zfp94, and is regulated by CASP8, a key component of apoptosis (Figure 5D).

Qualitative western blot analysis of vimentin and βB2-crystallin

We next used immunoblotting to determine whether the increase in βB2-crystallin and vimentin abundance occurred in the water-soluble or water-insoluble fraction of the lens. Water-soluble and water-insoluble fractions were obtained from the lens as described previously (23), then analyzed by SDS-PAGE and immunoblotting. Our results indicated that the increase in βB2-crystallin and vimentin expression in DKO lenses occurred in the water-insoluble fraction (Figure S5).

Qualitative assessment of the molecular weights of WT and DKO lens proteins

GPC analysis of water-soluble proteins from 7-day-old WT and 9-day-old DKO lenses is shown in Figure 6. The protein concentrations for the 7-day-old WT and 9-day-old DKO lenses were 1.87 and 1.15 mg/ml, respectively. The RI profile for the WT proteins revealed an α-crystallin peak at 12 ml. This α-crystallin peak is absent in the DKO proteins (Figure 6A). However, there is a new small, broader peak eluting at 13 ml in the DKO proteins (Figure 6A). This suggests that the β- and/or γ-crystallins may be aggregating into higher molecular weight, water-soluble species. Figure 6B shows the light scattering profile of proteins from 7- to 9-day-old lenses. The greatest light scattering in WT lenses occurs in the α-crystallin peak. In addition, WT proteins contain a high molecular weight peak that elutes in the void volume at 10 ml. This high molecular weight, water-soluble peak has been reported in human and bovine lenses (30–32). A smaller high molecular weight peak was also present in the void volume of DKO lenses (Figure 6B, Table 4). Both the molecular weight and intensity of the additional peak in the water-soluble proteins were lower than the WT high-molecular weight peak.

We next examined the water-soluble lens proteins of adult mice. Data for the RI and light scattering profiles of WT and DKO water-soluble proteins separated by GPC are shown in Figures 6C and 6D, respectively. Protein concentrations for water-soluble proteins from the lens of 117-day-old WT and 107-day-old DKO mice were 10 and 1.08 mg/ml, respectively. This indicates that soluble protein levels are greatly diminished in the 107-day-old DKO lenses compared with those in age-matched WT, 7 day-old WT, and 7-day-old DKO lenses. The light scattering profile of the 107-day-old WT α-crystallin fraction exhibited a major α-crystallin peak and smaller peaks for β- and γ-crystallins, similar to those observed in the 7-day-old WT lens, as well as a distinct shoulder with a molecular mass greater than that for the main α-crystallin fraction, suggesting that the molecular weight of the older WT α-crystallin is higher than that in the younger lens. This finding was also confirmed by the data analysis shown in Table 4. As expected, the α-crystallin peak was absent in the light scattering profile of DKO lenses (Figure 6D), but there was a small peak in the void volume of the adult DKO lens proteins The light scattering from β- and γ-crystallins was very low due to the low concentration of adult DKO water-soluble proteins, so the light scattering profile of DKO lenses is shown at a higher magnification in the inset of Figure 6D.

To determine whether the additional small peaks in soluble proteins from DKO lenses were artifacts, we next performed GPC at equal protein concentrations for WT and DKO lens proteins (Figure S6). In 9-day-old DKO lens proteins, there was a new peak eluting at 13 ml just after the WT α-crystallin peak, which eluted at 12.8 ml (Figure S6A). This new peak

was also present in the light scattering plot of younger lens proteins (Figure S6B). In adult DKO lens proteins, the RI plot exhibited a distinct shoulder at 15 ml just prior to the main β-crystallin peak at 16.5 ml (Figure S6C). In addition, in these adult DKO lens proteins, the light scattering plot revealed a new peak eluting at 10.5 ml in the void volume (Figure S6D), suggesting that some of the water-soluble β- and/or γ-crystallins have aggregated into high molecular weight species with a size > 10×10^6 Da. The data also indicated that the presence of this high molecular weight fraction in the RI profile of 9-day-old DKO lens proteins (Figure 6A) became water-insoluble with age, and was therefore not observed in the RI profile of 107-day-old DKO lens proteins (Figure S6C).

The molecular weight and hydrodynamic radius (R_h) of each of the water-soluble protein fractions were calculated (Table 4). Both WT and DKO β- and γ-crystallin proteins increased in both molecular weight and R_h with age. It is known that the composition of β- and γ-crystallin polypeptides changes with age (27). Thus, the change in the molecular weights of the β- and γ-crystallin fractions with age in WT lenses may be due to the expression of new polypeptides with aging. The molecular weights of β-and γ-crystallin peaks in DKO lenses were higher than those of age-matched WT lenses (Table 4). The molecular weight of the water-soluble α-crystallin fraction was 682 kDa in 7-day-old WT lenses, which increased to 1141 kDa in 117-day-old WT lenses. There was no α-crystallin peak detected in DKO lenses. However, a new peak with a molecular weight of 328 kDa was detected in 9-day-old DKO lens proteins, and a shoulder with a molecular weight of 298 kDa was observed in the 107-day-old DKO proteins.

We hypothesize that these new protein species resulted from aggregation of β-crystallin into higher than normal molecular weight species in DKO lenses. We therefore used western blots of protein fractions collected from the GPC column to determine the identity of these new peaks. Immunoblot analysis revealed that the new peak contained a protein reactive with β-crystallin antibodies but not with a γ-crystallin antibody, indicating that at least part of the higher molecular weight protein species was aggregated β-crystallin. The protein in this peak cross-reacted with an antibody specific for β-crystallin (Figure S7). This suggests that the new peak with a molecular mass of 328 kDa in 1-week-old DKO lenses was created by the aggregation of β-crystallin polypeptides into high molecular weight aggregates. As expected, the new 328 kDa proteins in 9-day-old DKO lenses contained β-crystallin but not α- or γ-crystallin (data not shown). The new 298 kDa protein shoulder in the 107-day-old DKO lenses contained both β- and γ-crystallin (data not shown). This analysis revealed that in the absence of α-crystallins, β- and γ-crystallin aggregated in DKO lenses into high molecular weight proteins.

Changes in protein abundance of βB2-crystallin and vimentin could have occurred at the transcriptional level due to increases in the transcription of these proteins. Therefore, we determined the mRNA expression of the genes encoding these proteins by quantitative PCR using gene-specific primers (Figure S8). The mRNA abundances were similar in WT and DKO lenses (Figure S8), indicating that the protein increases we observed are not due to increased mRNA transcription.

Discussion

The α-crystallins are molecular chaperones that are known to exhibit anti-apoptotic properties (5, 13, 33). Although expressed at other sites in the body, αA-crystallin is found in largest amounts in mammalian lenses, whereas αB-crystallin is present almost ubiquitously (34). Lens epithelial and cortical fiber cells from normal lenses express large amounts of αA- and αB-crystallin (10, 35). DKO mice are born with cataracts and significant morphological defects (36), which have been attributed to loss of α-crystallin

chaperone availability, resulting in increases in protein insolubilization and light scattering of high molecular weight protein aggregates, activation of caspases, and apoptotic cell death (13). However, lens proteomic changes resulting from the loss of the α-crystallins have not been described. In this study, we show that some of the earliest observable changes in DKO mouse lenses involve cross-linking of βB1-crystallin (increase in βB1-crystallin spot 3027), degradation of β1-catenin to 11–14 kDa fragments (increase in spots 6171, 6278, 6308, 6463, 6502, 6696, 7235, 1093, and 6908), and increase in relative abundance of histones (spots 6278, 6308, 6463, 6502, and 6696). Histones were associated with many of the spots containing β1-catenin. Our analyses indicated that degradation of β1-catenin, cross-linking of βB1-crystallin, and increased amounts of histones are the earliest changes in DKO lenses, suggesting that α-crystallins may be a chaperone for β1-catenin and βB1-crystallin, and that α-crystallins may regulate the expression of histones. Our analyses also implicate networks that are altered in the absence of αA- and αB-crystallin in the lens, which can be used to generate and experimentally test new hypotheses for the biological significance of these chaperones.

Several important experimental results of this study require further discussion. We used image analysis to quantify the abundance of each protein spot. The analysis quantifies the intensity within the largest footprint of the boundary for a spot on a gel containing proteins from three different samples. Thus, even though αA- and αB-crystallin have been deleted from the DKO sample, the DKO sample will still have an intensity value assigned to it, which represents the background of the empty spot in the DKO sample. Crystallins are expressed in large amounts in the lens, and their concentration increases significantly between postnatal day 2 and adult lens. The use of lens epithelial fractions allowed the analysis of lower abundance proteins in adult lenses by 2D-DIGE- and LC/MS/MS-based proteomics. This proteomic analysis also demonstrated increased abundance of βB2-crystallin and vimentin in lens epithelial fractions. The increase in abundance of βB2-crystallin in epithelial fractions was also detected in the fiber cell fractions (data not shown).

Our findings showing elevations in histones and low molecular weight β1-catenin in the postnatal lens are of particular importance. β-Catenin is also a cell adhesion protein and is associated with N-cadherin in adherens junctions between lens fiber cells, and therefore may play a role in maintaining these junctions during lens development (37, 38). These N-cadherin junctions are a prominent feature of lateral interfaces of undifferentiated lens epithelial cells and are important for the assembly of the actin cytoskeleton during fiber cell elongation (38). β1-catenin is also a nuclear transcription regulator. Alterations in β1-catenin, suggested by the loss of intact β-catenin in DKO lenses at early stages when key developmental events are occurring may indicate the potential role of α-crystallins in this process. Lastly, Wnt signaling is important in lens development and morphogenesis, and our findings support previous studies in which disruption of normal Wnt signaling has been linked with cataract formation in several model systems (38–41).

The present study demonstrates an increase in histones in the absence of α-crystallins and suggests that α-crystallins regulate the binding of histones to DNA in vivo. The association of histones and β-catenin in a number of protein spots (6278, 6308, 6463, 6502, and 6696, Table 1) suggests that α-crystallins may regulate the recruitment of histones which in turn regulate the Wnt-β-catenin signaling pathway. The association of histones and Wnt signaling has been demonstrated to be a mode of regulation of the Wnt signaling pathway (42). Previous work in our laboratory used mass spectrometry to identify histones 2B (~13.94 kDa) and H4 (~11 kDa) in co-immunoprecipitates of lens epithelial cell α-crystallins (43). The abundance of these αA-crystallin-associated histones increased in the R116C mutation of αA-crystallin. The increased abundance of histones observed in postnatal day 2 DKO lenses also suggests that a small amount of α-crystallins may be

present in the nucleus. αA-crystallins have been shown to undergo phosphorylation in vivo and act as an autokinase (6). The phosphorylation of certain histones is dependent on the activation of caspases, and therefore may be linked to caspase activation observed in DKO lenses (13). Histone H2B undergoes phosphorylation in response to apoptotic signals in mammalian cells, which may facilitate access of damaged DNA to repair mechanisms (44, 45). It has also been reported that histone transcripts accumulate with exposure of lens epithelial cells to ultraviolet C radiation (46). The possible association of αA-and αB-crystallin with histones is also consistent with their involvement in cell growth (9, 11).

We further demonstrated that the absence of α-crystallins increases the amount of vimentin crosslinked with tubulin. Proteins were analyzed in the presence of urea, therefore the association of vimentin and tubulin indicates that the proteins in these spots are covalently linked. We did not observe a significant increase in vimentin mRNA in DKO lenses. Increased vimentin expression has also been reported in HSF4 knockout mice, and has been demonstrated to be due to the loss of HSF4 binding to the vimentin promoter that normally represses vimentin expression (47).

Human, mouse, rat, and zebrafish lenses have been extensively analyzed by proteomic approaches (27, 30–32, 48–52). Studies have shown that intact α-crystallins decline with age in human lenses, and fragments of α-, βB1, and γS-crystallin have been identified in human lens protein extracts (53). In addition, βB1-crystallin degradation and truncation with aging is believed to increase light scattering in the lens (54). Our finding of cross-linked βB1-crystallin identified in DKO lenses (Figure 1 and Table 1) suggests that it may be one of the factors resulting in opacities in these lenses (13, 36).

Alterations in proteins of the proteasomal machinery in the DKO lens may be particularly important. Previous studies reported that αB-crystallin acts as a chaperone in targeting proteins to the ubiquitin-proteasome system for degradation (55). Our study demonstrated that with the loss of α-crystallin there is an increase in the abundance of an ubiquitin-like protein and the proteasome activator complex 2. In addition, the abundance of endoplasmic reticulum protein 29 in DKO3 lenses was 4-fold greater when compared with WT6 lenses (Table 3).

The results presented in this study showed not only changes in relative abundances of crystallins, but also showed changes in relative abundances of several enzymes and proteins, including titin and hemoglobin subunit α, plus a decrease in DKO lenses of the enzymes glucose-6-phosphate isomerase, retinal dehydrogenase 1, glutamate dehydrogenase and ATP synthetase. These proteins are involved in maintenance of lens metabolism and resistance against oxidative stress. The abundances in protein spots containing the enzymes glucose 6-phosphate isomerase and retinal dehydrogenase 1 (spot 2789) decreased nearly 6-fold in DKO lenses. The expression of retinal dehydrogenase 1 has recently been reported to decrease in human nuclear cataracts (56) and UVB-irradiated human lenses (57), indicating common mechanisms in two other cataract models and suggesting that its decreased abundance may be related to increased stress. The origin of the observed increase in GSTfamily members in DKO lenses is unclear at present.

The increase in molecular weights of β- and γ-crystallin fractions in DKO lenses identified in this study is of particular importance, because it could disrupt the normal short-range order and increase protein insolubilization in DKO lenses. Our data also demonstrated that the relative abundance of water-soluble protein decreased nearly 10-fold in adult DKO lenses compared to that in age-matched WT controls. Furthermore, changes in β-crystallin were observed at an early age. βB2-crystallin formed high molecular weight, water-soluble aggregates of approximately 328 kDa in 9-day-old DKO lenses that were absent in age-

matched WT lenses. The absence of the 328 kDa peak in the adult DKO lenses in GPC analysis indicated that this protein becomes increasingly aggregated into water-insoluble, high molecular weight aggregates with age. It has been reported that the amount of water-insoluble crystallins increases with age of the lens and with human cataract formation (58). The proposed sequence of events involves conversion of water-soluble proteins to high molecular weight, water-soluble proteins that increase in molecular weight and subsequently become water-insoluble (59). Our GPC data are consistent with this hypothesis in DKO lenses. Thus, our data suggest that the DKO lens is a good model for the study of protein alterations in human lens aging and cataract formation.

The increase in βB2-crystallin abundance observed in the 35-day-old lens epithelial fractions was novel and unexpected, and the present study determined that this increase occurred in the water-insoluble fraction. The monomer molecular weight of βB2-crystallin is 24 kDa, but it readily forms a homodimer as well as heterodimers and heterooctamers with other β-crystallin subunits (49, 60–65). We found that the abundances of βA3/A1- and βS-crystallin decreased, whereas that of βB3-crystallin increased, in spots containing multiple proteins in DKO lenses (Table 3). The βB2-crystallin gene is expressed late in the lens, being expressed in mice only in the postnatal lens (27, 66, 67). Targeted knockout of the mouse βB2-crystallin gene induces cataract formation in adult mice (68), and one of its mutations has been linked to infertility in mice (69–71). βB2-crystallin is also expressed in the retina, and axonal regeneration appears linked to βB2-crystallin (72). Together, these results support the concept that βB2-crystallin has non-refractive functions and may serve a protective role in the lens. Further studies are necessary to fully understand the relevance of increased βB2-crystallin resulting from loss of α-crystallins as one of its major chaperones.

In summary, our proteomic analysis identified several novel candidates that may be substrates for α-crystallin protection. These proteins will be further investigated for their relationship to lens defects and to α-crystallin function in vivo. Furthermore, similar studies can be used to characterize the function of α-crystallins in tissues such as muscle, where αB-crystallin is expressed in abundance. For example, titin is a multifunctional protein that is decreased 3-fold in DKO lenses. Because titin is a major component of muscle fibers and is known to associate with αB-crystallin, this finding is of particular importance to muscle physiology (73, 74). Our study provides a compendium of proteins whose expression is altered in response to the absence of α-crystallins in mouse lenses. Proteins identified by us can be organized into several key networks including those involving adherens junctions, cytoskeleton, chaperones, and cell signaling, providing the basis for future mechanistic studies. We propose that the profound changes in proteins known to regulate the cytoskeleton, cell adhesion, and specific metabolic pathways could result in long-lasting structural and functional lens defects. Of particular interest will be a further understanding of the extent to which these proteins represent in vivo substrates for α-crystallin function, possibly involving metabolic pathways protected and regulated by this small heat shock protein.

Supplementary Material

Refer to Web version on PubMed Central for supplementary material.

Acknowledgments

The authors thank Petra Gilmore and Matthew Bartley for expert technical assistance.

Supported by the National Institutes of Health (NIH) grant R01EY05681 to UPA, Core Grant EY02687, Research to Prevent Blindness grants to the Department of Ophthalmology and Visual Sciences at Washington University School of Medicine, Washington University Institute of Clinical and Translational Sciences grant UL1 TR000448

from the National Center for Advancing Translational Sciences (NCATS) of the NIH, grants from the National Center for Research Resources (5P41RR000954-35), and the National Institute of General Medical Sciences (8 P41 GM103422-35) from the NIH. The content is solely the responsibility of the authors and does not necessarily represent the official view of the NIH.

Abbreviations

WT	wild-type
DKO	double knockout
SDS-PAGE	sodium dodecyl sulfate-polyacrylamide gel electrophoresis
GPC	gel permeation chromatography
2D-DIGE	two-dimensional difference gel electrophoresis
RT-PCR	reverse transcriptase-polymerase chain reaction
RI	refractive index
PBS	phosphate-buffered saline
$\mathbf{R_h}$	hydrodynamic radius

REFERENCES

1. Benedek GB. Theory of transparency of the eye. Appl. Optics. 1971; 10:459–473.
2. Robinson ML, Overbeek PA. Differential expression of alpha A- and alpha B-crystallin during murine ocular development. Invest Ophthalmol Vis Sci. 1996; 37:2276–2284. [PubMed: 8843924]
3. Piatigorsky J. Lens differentiation in vertebrates. A review of cellular and molecular features. Differentiation. 1981; 19:134–153. [PubMed: 7030840]
4. Bloemendal H, de Jong W, Jaenicke R, Lubsen NH, Slingsby C, Tardieu A. Ageing and vision: structure, stability and function of lens crystallins. Prog Biophys Mol Biol. 2004; 86:407–485. [PubMed: 15302206]
5. Horwitz J. Alpha-crystallin can function as a molecular chaperone. Proc Natl Acad Sci U S A. 1992; 89:10449–10453. [PubMed: 1438232]
6. Kantorow M, Piatigorsky J. Alpha-crystallin/small heat shock protein has autokinase activity. Proc Natl Acad Sci U S A. 1994; 91:3112–3116. [PubMed: 8159713]
7. Brady JP, Garland D, Duglas-Tabor Y, Robison WG Jr, Groome A, Wawrousek EF. Targeted disruption of the mouse alpha A-crystallin gene induces cataract and cytoplasmic inclusion bodies containing the small heat shock protein alpha B-crystallin. Proc Natl Acad Sci U S A. 1997; 94:884–889. [PubMed: 9023351]
8. Brady JP, Garland DL, Green DE, Tamm ER, Giblin FJ, Wawrousek EF. AlphaB-crystallin in lens development and muscle integrity: a gene knockout approach. Invest Ophthalmol Vis Sci. 2001; 42:2924–2934. [PubMed: 11687538]
9. Andley UP, Song Z, Wawrousek EF, Bassnett S. The molecular chaperone alphaA-crystallin enhances lens epithelial cell growth and resistance to UVA stress. J Biol Chem. 1998; 273:31252–31261. [PubMed: 9813033]
10. Xi JH, Bai F, Andley UP. Reduced survival of lens epithelial cells in the alphaA-crystallin-knockout mouse. J Cell Sci. 2003; 116:1073–1085. [PubMed: 12584250]
11. Andley UP, Song Z, Wawrousek EF, Brady JP, Bassnett S, Fleming TP. Lens epithelial cells derived from alphaB-crystallin knockout mice demonstrate hyperproliferation and genomic instability. Faseb J. 2001; 15:221–229. [PubMed: 11149910]
12. Bai F, Xi JH, Wawrousek EF, Fleming TP, Andley UP. Hyperproliferation and p53 status of lens epithelial cells derived from alphaB-crystallin knockout mice. J Biol Chem. 2003; 278:36876–36886. [PubMed: 12826669]

13. Morozov V, Wawrousek EF. Caspase-dependent secondary lens fiber cell disintegration in alphaA-/alphaB-crystallin double-knockout mice. Development. 2006; 133:813–821. [PubMed: 16439475]
14. Bai F, Xi J, Higashikubo R, Andley UP. Cell kinetic status of mouse lens epithelial cells lacking alphaA- and alphaB-crystallin. Mol Cell Biochem. 2004; 265:115–122. [PubMed: 15543941]
15. Bai F, Xi JH, Andley UP. Up-regulation of tau, a brain microtubule-associated protein, in lens cortical fractions of aged alphaA-, alphaB-, and alphaA/B-crystallin knockout mice. Mol Vis. 2007; 13:1589–1600. [PubMed: 17893660]
16. Cao Y, Cheong H, Song H, Klionsky DJ. In vivo reconstitution of autophagy in Saccharomyces cerevisiae. J Cell Biol. 2008; 182:703–713. [PubMed: 18725539]
17. Xi JH, Bai F, McGaha R, Andley UP. Alpha-crystallin expression affects microtubule assembly and prevents their aggregation. Faseb J. 2006; 20:846–857. [PubMed: 16675842]
18. Nicholl ID, Quinlan RA. Chaperone activity of alpha-crystallins modulates intermediate filament assembly. Embo J. 1994; 13:945–953. [PubMed: 7906647]
19. Perng MD, Muchowski PJ, van Den IP, Wu GJ, Hutcheson AM, Clark JI, Quinlan RA. The cardiomyopathy and lens cataract mutation in alphaB crystallin alters its protein structure, chaperone activity, and interaction with intermediate filaments in vitro. J Biol Chem. 1999; 274:33235–33243. [PubMed: 10559197]
20. McHaourab HS, Kumar MS, Koteiche HA. Specificity of alphaA-crystallin binding to destabilized mutants of betaB1-crystallin. FEBS Lett. 2007; 581:1939–1943. [PubMed: 17449033]
21. Mendelsohn BA, Malone JP, Townsend RR, Gitlin JD. Proteomic analysis of anoxia tolerance in the developing zebrafish embryo. Comp Biochem Physiol Part D Genomics Proteomics. 2009; 4:21–31. [PubMed: 20403745]
22. Morales DM, Townsend RR, Malone JP, Ewersmann CA, Macy EM, Inder TE, Limbrick DD Jr. Alterations in protein regulators of neurodevelopment in the cerebrospinal fluid of infants with posthemorrhagic hydrocephalus of prematurity. Mol Cell Proteomics. 2012; 11:M111 011973. [PubMed: 22186713]
23. Chen J, Ma Z, Jiao X, Fariss R, Kantorow WL, Kantorow M, Pras E, Frydman M, Pras E, Riazuddin S, Riazuddin SA, Hejtmancik JF. Mutations in FYCO1 cause autosomal-recessive congenital cataracts. Am J Hum Genet. 2011; 88:827–838. [PubMed: 21636066]
24. Andley UP, Hamilton PD, Ravi N. Mechanism of insolubilization by a single-point mutation in alphaA-crystallin linked with hereditary human cataracts. Biochemistry. 2008; 47:9697–9706. [PubMed: 18700785]
25. Andley UP, Hamilton PD, Ravi N, Weihl CC. A knock-in mouse model for the R120G mutation of alphaB-crystallin recapitulates human hereditary myopathy and cataracts. PLoS ONE. 2011; 6:e17671. [PubMed: 21445271]
26. Andley UP, Patel HC, Xi JH, Bai F. Identification of genes responsive to UV-A radiation in human lens epithelial cells using complementary DNA microarrays. Photochem Photobiol. 2004; 80:61–71. [PubMed: 15339208]
27. Ueda Y, Duncan MK, David LL. Lens proteomics: the accumulation of crystallin modifications in the mouse lens with age. Invest Ophthalmol Vis Sci. 2002; 43:205–215. [PubMed: 11773033]
28. Dirscherl SS, Henry JJ, Krebs JE. Neural and eye-specific defects associated with loss of the imitation switch (ISWI) chromatin remodeler in Xenopus laevis. Mech Dev. 2005; 122:1157–1170. [PubMed: 16169710]
29. Cvekl A, Duncan MK. Genetic and epigenetic mechanisms of gene regulation during lens development. Prog Retin Eye Res. 2007; 26:555–597. [PubMed: 17905638]
30. Hoehenwarter W, Klose J, Jungblut PR. Eye lens proteomics. Amino acids. 2006; 30:369–389. [PubMed: 16583312]
31. Wilmarth PA, Riviere MA, David LL. Techniques for accurate protein identification in shotgun proteomic studies of human, mouse, bovine, and chicken lenses. Journal of ocular biology, diseases, and informatics. 2009; 2:223–234.
32. Andley UP, Malone JP, Townsend RR. Inhibition of lens photodamage by UV-absorbing contact lenses. Invest Ophthalmol Vis Sci. 2011; 52:8330–8341. [PubMed: 21873653]

33. Andley UP, Song Z, Wawrousek EF, Fleming TP, Bassnett S. Differential protective activity of alpha A- and alphaB-crystallin in lens epithelial cells. J Biol Chem. 2000; 275:36823–36831. [PubMed: 10967101]
34. Sax CM, Piatigorsky J. Expression of the alpha-crystallin/small heat-shock protein/molecular chaperone genes in the lens and other tissues. Adv Enzymol Relat Areas Mol Biol. 1994; 69:155–201. [PubMed: 7817868]
35. Wang X, Garcia CM, Shui YB, Beebe DC. Expression and regulation of alpha-, beta-, and gamma-crystallins in mammalian lens epithelial cells. Invest Ophthalmol Vis Sci. 2004; 45:3608–3619. [PubMed: 15452068]
36. Boyle DL, Takemoto L, Brady JP, Wawrousek EF. Morphological characterization of the Alpha A- and Alpha B-crystallin double knockout mouse lens. BMC Ophthalmol. 2003; 3:3. [PubMed: 12546709]
37. Munafo DB, Colombo MI. A novel assay to study autophagy: regulation of autophagosome vacuole size by amino acid deprivation. J Cell Sci. 2001; 114:3619–3629. [PubMed: 11707514]
38. Seglen PO, Berg TO, Blankson H, Fengsrud M, Holen I, Stromhaug PE. Structural aspects of autophagy. Adv Exp Med Biol. 1996; 389:103–111. [PubMed: 8860999]
39. Gilliland KO, Freel CD, Johnsen S, Craig Fowler W, Costello MJ. Distribution, spherical structure and predicted Mie scattering of multilamellar bodies in human age-related nuclear cataracts. Exp Eye Res. 2004; 79:563–576. [PubMed: 15381040]
40. Hariri M, Millane G, Guimond MP, Guay G, Dennis JW, Nabi IR. Biogenesis of multilamellar bodies via autophagy. Mol Biol Cell. 2000; 11:255–268. [PubMed: 10637306]
41. Bettelheim FA. Light scattering in lens research: an essay on accomplishments and promises. Exp Eye Res. 2004; 79:747–752. [PubMed: 15642311]
42. Nishiyama M, Skoultchi AI, Nakayama KI. Histone H1 recruitment by CHD8 is essential for suppression of the Wnt-beta-catenin signaling pathway. Mol Cell Biol. 2012; 32:501–512. [PubMed: 22083958]
43. Andley UP, Patel HC, Xi JH. The R116C mutation in alpha A-crystallin diminishes its protective ability against stress-induced lens epithelial cell apoptosis. J Biol Chem. 2002; 277:10178–10186. [PubMed: 11756414]
44. Moncaster JA, Pineda R, Moir RD, Lu S, Burton MA, Ghosh JG, Ericsson M, Soscia SJ, Mocofanescu A, Folkerth RD, Robb RM, Kuszak JR, Clark JI, Tanzi RE, Hunter DG, Goldstein LE. Alzheimer's disease amyloid-beta links lens and brain pathology in Down syndrome. PLoS ONE. 2010; 5:e10659. [PubMed: 20502642]
45. Muchowski PJ, Ramsden R, Nguyen Q, Arnett EE, Greiling TM, Anderson SK, Clark JI. Noninvasive measurement of protein aggregation by mutant huntingtin fragments or alpha-synuclein in the lens. J Biol Chem. 2008; 283:6330–6336. [PubMed: 18167346]
46. Sidjanin D, Grdina D, Woloschak GE. UV-induced changes in cell cycle and gene expression within rabbit lens epithelial cells. Photochem. Photobiol. 1996; 63:79–85. [PubMed: 8577869]
47. Brennan LA, Kantorow WL, Chauss D, McGreal R, He S, Mattucci L, Wei J, Riazuddin SA, Cvekl A, Hejtmancik JF, Kantorow M. Spatial expression patterns of autophagy genes in the eye lens and induction of autophagy in lens cells. Mol Vis. 2012; 18:1773–1786. [PubMed: 22815631]
48. Grey AC, Schey KL. Age-related Changes in the Spatial Distribution of Human Lens {alpha}-Crystallin Products by MALDI Imaging Mass Spectrometry. Invest Ophthalmol Vis Sci. 2009
49. Lampi KJ, Ma Z, Hanson SR, Azuma M, Shih M, Shearer TR, Smith DL, Smith JB, David LL. Age-related changes in human lens crystallins identified by two-dimensional electrophoresis and mass spectrometry. Exp Eye Res. 1998; 67:31–43. [PubMed: 9702176]
50. Lampi KJ, Shih M, Ueda Y, Shearer TR, David LL. Lens proteomics: analysis of rat crystallin sequences and two-dimensional electrophoresis map. Invest Ophthalmol Vis Sci. 2002; 43:216–224. [PubMed: 11773034]
51. Greiling TM, Houck SA, Clark JI. The zebrafish lens proteome during development and aging. Mol Vis. 2009; 15:2313–2325. [PubMed: 19936306]
52. Posner M, Hawke M, Lacava C, Prince CJ, Bellanco NR, Corbin RW. A proteome map of the zebrafish (Danio rerio) lens reveals similarities between zebrafish and mammalian crystallin expression. Mol Vis. 2008; 14:806–814. [PubMed: 18449354]

53. Su SP, McArthur JD, Truscott RJ, Aquilina JA. Truncation, cross-linking and interaction of crystallins and intermediate filament proteins in the aging human lens. Biochim Biophys Acta. 2011; 1814:647–656. [PubMed: 21447408]
54. Annunziata O, Pande A, Pande J, Ogun O, Lubsen NH, Benedek GB. Oligomerization and phase transitions in aqueous solutions of native and truncated human beta B1-crystallin. Biochemistry. 2005; 44:1316–1328. [PubMed: 15667225]
55. den Engelsman J, Keijsers V, de Jong WW, Boelens WC. The small heat-shock protein alpha B-crystallin promotes FBX4-dependent ubiquitination. J Biol Chem. 2003; 278:4699–4704. [PubMed: 12468532]
56. Cheong H, Nair U, Geng J, Klionsky DJ. The Atg1 kinase complex is involved in the regulation of protein recruitment to initiate sequestering vesicle formation for nonspecific autophagy in Saccharomyces cerevisiae. Mol Biol Cell. 2008; 19:668–681. [PubMed: 18077553]
57. Bettelheim FA, Li L, Zeng FF. Do changes in the hydration of the diabetic human lens precede cataract formation? Research communications in molecular pathology and pharmacology. 1998; 102:3–14. [PubMed: 9920342]
58. Liang JN, Andley UP, Chylack LT Jr. Spectroscopic studies on human lens crystallins. Biochim Biophys Acta. 1985; 832:197–203. [PubMed: 4063377]
59. Andley UP, LJ.; Lou, MF. Biochemical mechanisms of age-related cataract. 2nd ed. Vol. Vol. 2. Philadelphia, PA: WB Saunders; 2000.
60. Lee HS, Daniels BH, Salas E, Bollen AW, Debnath J, Margeta M. Clinical utility of LC3 and p62 immunohistochemistry in diagnosis of drug-induced autophagic vacuolar myopathies: a case-control study. PLoS ONE. 2012; 7:e36221. [PubMed: 22558391]
61. Komatsu M, Waguri S, Koike M, Sou YS, Ueno T, Hara T, Mizushima N, Iwata J, Ezaki J, Murata S, Hamazaki J, Nishito Y, Iemura S, Natsume T, Yanagawa T, Uwayama J, Warabi E, Yoshida H, Ishii T, Kobayashi A, Yamamoto M, Yue Z, Uchiyama Y, Kominami E, Tanaka K. Homeostatic levels of p62 control cytoplasmic inclusion body formation in autophagy-deficient mice. Cell. 2007; 131:1149–1163. [PubMed: 18083104]
62. Moscat J, Diaz-Meco MT, Wooten MW. Signal integration and diversification through the p62 scaffold protein. Trends Biochem Sci. 2007; 32:95–100. [PubMed: 17174552]
63. Choi JC, Muchir A, Wu W, Iwata S, Homma S, Morrow JP, Worman HJ. Temsirolimus activates autophagy and ameliorates cardiomyopathy caused by lamin a/c gene mutation. Science translational medicine. 2012; 4:144ra102.
64. Martinez-Vicente M, Talloczy Z, Wong E, Tang G, Koga H, Kaushik S, de Vries R, Arias E, Harris S, Sulzer D, Cuervo AM. Cargo recognition failure is responsible for inefficient autophagy in Huntington's disease. Nature neuroscience. 2010; 13:567–576.
65. Lampi KJ, Amyx KK, Ahmann P, Steel EA. Deamidation in human lens betaB2-crystallin destabilizes the dimer. Biochemistry. 2006; 45:3146–3153. [PubMed: 16519509]
66. Beebe DC, Vasiliev O, Guo J, Shui YB, Bassnett S. Changes in adhesion complexes define stages in the differentiation of lens fiber cells. Invest Ophthalmol Vis Sci. 2001; 42:727–734. [PubMed: 11222534]
67. Chambers C, Russell P. Deletion mutation in an eye lens beta-crystallin. An animal model for inherited cataracts. J Biol Chem. 1991; 266:6742–6746. [PubMed: 1707874]
68. Zhang J, Li J, Huang C, Xue L, Peng Y, Fu Q, Gao L, Zhang J, Li W. Targeted knockout of the mouse betaB2-crystallin gene (Crybb2) induces age-related cataract. Invest Ophthalmol Vis Sci. 2008; 49:5476–5483. [PubMed: 18719080]
69. Duprey KM, Robinson KM, Wang Y, Taube JR, Duncan MK. Subfertility in mice harboring a mutation in betaB2-crystallin. Mol Vis. 2007; 13:366–373. [PubMed: 17392687]
70. Santhiya ST, Manisastry SM, Rawlley D, Malathi R, Anishetty S, Gopinath PM, Vijayalakshmi P, Namperumalsamy P, Adamski J, Graw J. Mutation analysis of congenital cataracts in Indian families: identification of SNPS and a new causative allele in CRYBB2 gene. Invest Ophthalmol Vis Sci. 2004; 45:3599–3607. [PubMed: 15452067]
71. Litt M, Carrero-Valenzuela R, LaMorticella DM, Schultz DW, Mitchell TN, Kramer P, Maumenee IH. Autosomal dominant cerulean cataract is associated with a chain termination mutation in the

human beta-crystallin gene CRYBB2. Human molecular genetics. 1997; 6:665–668. [PubMed: 9158139]

72. Liedtke T, Schwamborn JC, Schroer U, Thanos S. Elongation of axons during regeneration involves retinal crystallin beta b2 (crybb2). Mol Cell Proteomics. 2007; 6:895–907. [PubMed: 17264069]
73. Bullard B, Ferguson C, Minajeva A, Leake MC, Gautel M, Labeit D, Ding L, Labeit S, Horwitz J, Leonard KR, Linke WA. Association of the chaperone alphaB-crystallin with titin in heart muscle. J Biol Chem. 2004; 279:7917–7924. [PubMed: 14676215]
74. Golenhofen N, Htun P, Ness W, Koob R, Schaper W, Drenckhahn D. Binding of the stress protein alpha B-crystallin to cardiac myofibrils correlates with the degree of myocardial damage during ischemia/reperfusion in vivo. J Mol Cell Cardiol. 1999; 31:569–580. [PubMed: 10198188]

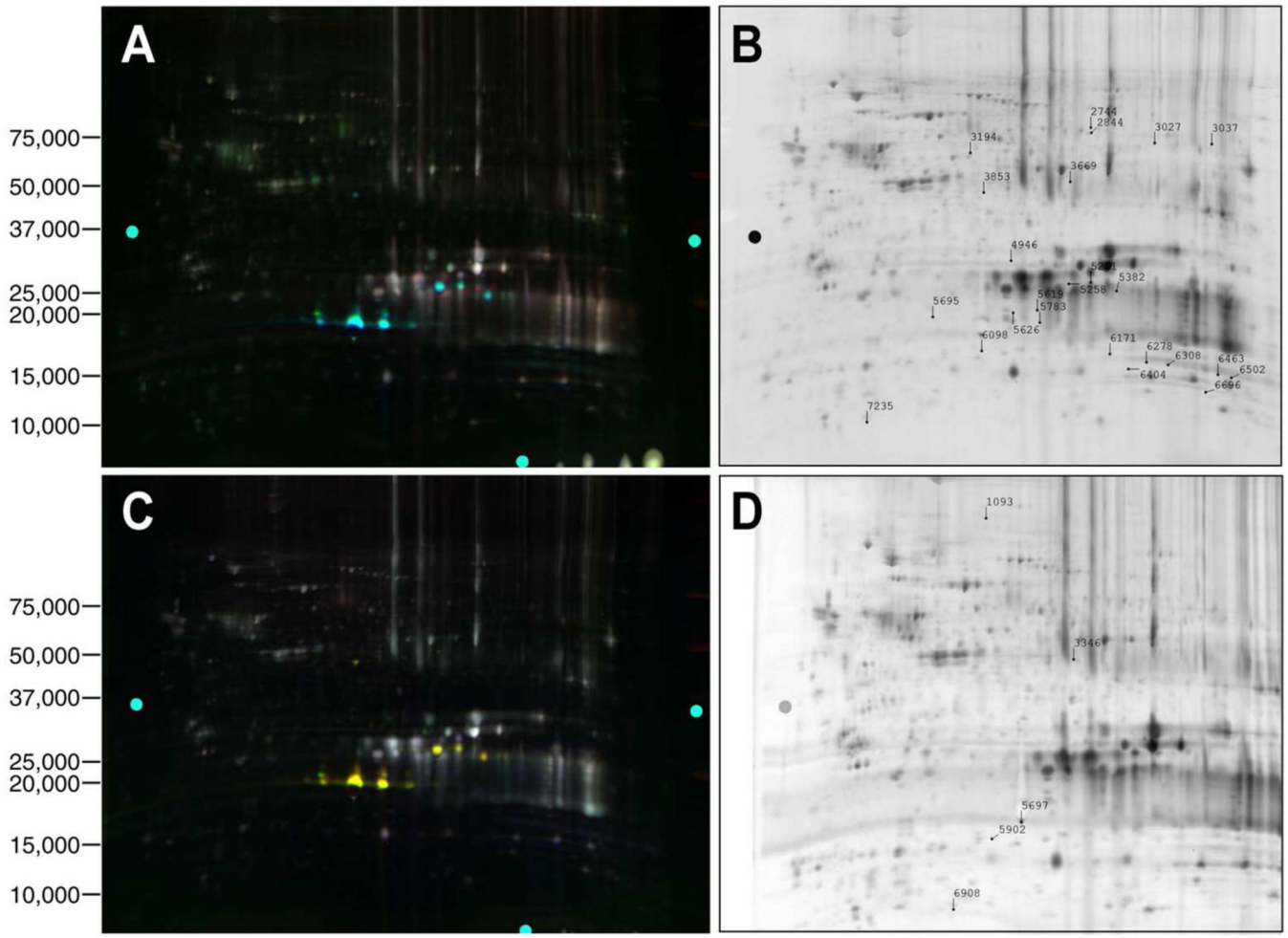

Figure 1.

The 2D-DIGE analysis of proteomic changes in whole lenses of 2-day-old mice induced by αA- and αB-crystallin gene deletions. (A) A 2D gel of lens proteins labeled with cyanine dyes derived from WT1 proteins labeled with Cy3, WT2 proteins labeled with Cy5, and DKO1 proteins labeled with Cy2. (B) Protein spots that were picked for analysis from the gel shown in (A). (C) A 2D gel of lens proteins labeled with cyanine dyes derived from WT3 proteins labeled with Cy2, WT4 proteins labeled with Cy3, and DKO2 proteins labeled with Cy5. (D) Protein spots that were picked for analysis from the gel shown in (C). Proteins were identified by tandem mass spectrometry and Mascot searches of spots that were differentially expressed. Quantitative image analysis and mass spectrometry data for identified proteins from this gel are listed in Table 1.

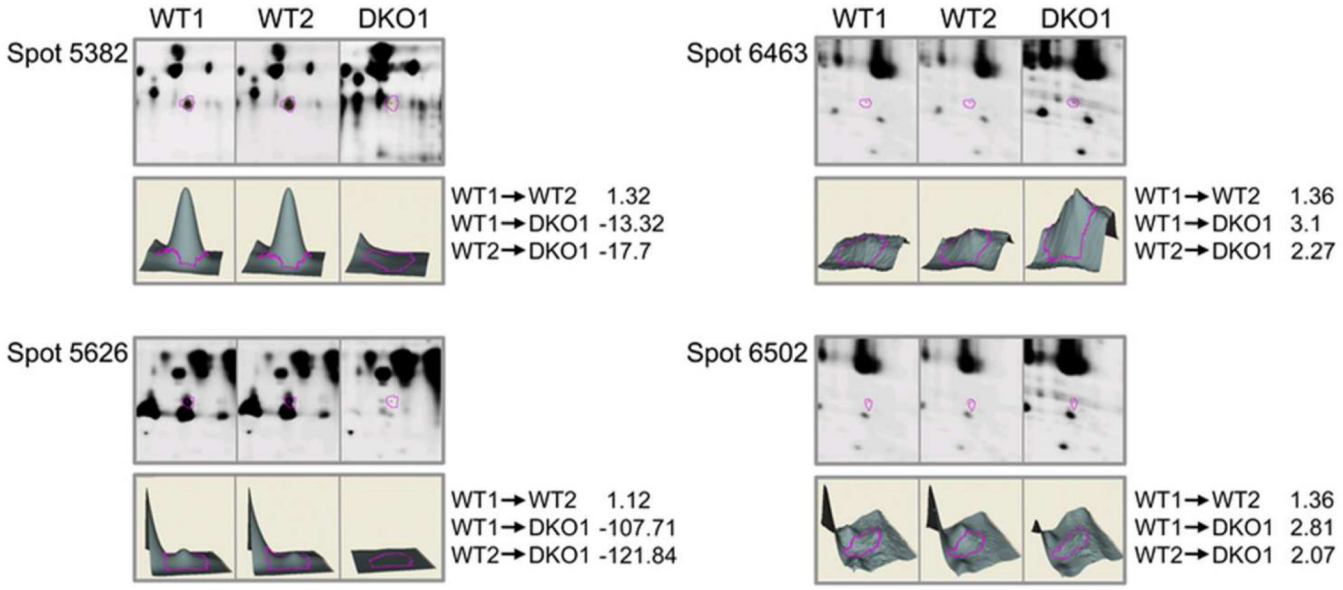

Figure 2.

(A) Quantitative analysis of changes in abundance of postnatal 2-day-old lens protein spots in WT and DKO lenses by mass spectrometry. The 3D data sets for representative proteins in two WT (WT1 and WT2) and one DKO (DKO1) sample are shown. DKO1 proteins were labeled with Cy2, WT1 proteins with Cy3, and WT2 proteins with Cy5 dyes. Fold changes between each sample are indicated on the right. See Table 1 for the identity of proteins present in each protein spot.

Figure 3.

(A) The 2D-DIGE analysis of proteomic changes in 70-day-old WT (WT5), 35-day-old WT (WT6), and 30-day-old DKO (DKO3) mouse lens epithelial fractions. A 2D gel of lens epithelial cell proteins labeled with cyanine dyes derived from WT5 proteins labeled with Cy2, WT6 proteins labeled with Cy3, and DKO3 proteins labeled with Cy5. Proteins were identified by tandem mass spectrometry and Mascot searches of spots that were differentially expressed. See Materials and Methods for additional details. (B) Protein spots that were picked for analysis are shown. Quantitative image analysis and mass spectrometry data for identified proteins from this gel are listed in Table 2. (C) Additional protein spots that were picked for analysis are shown. Identification of proteins in the analyzed spots is shown in Table 3.

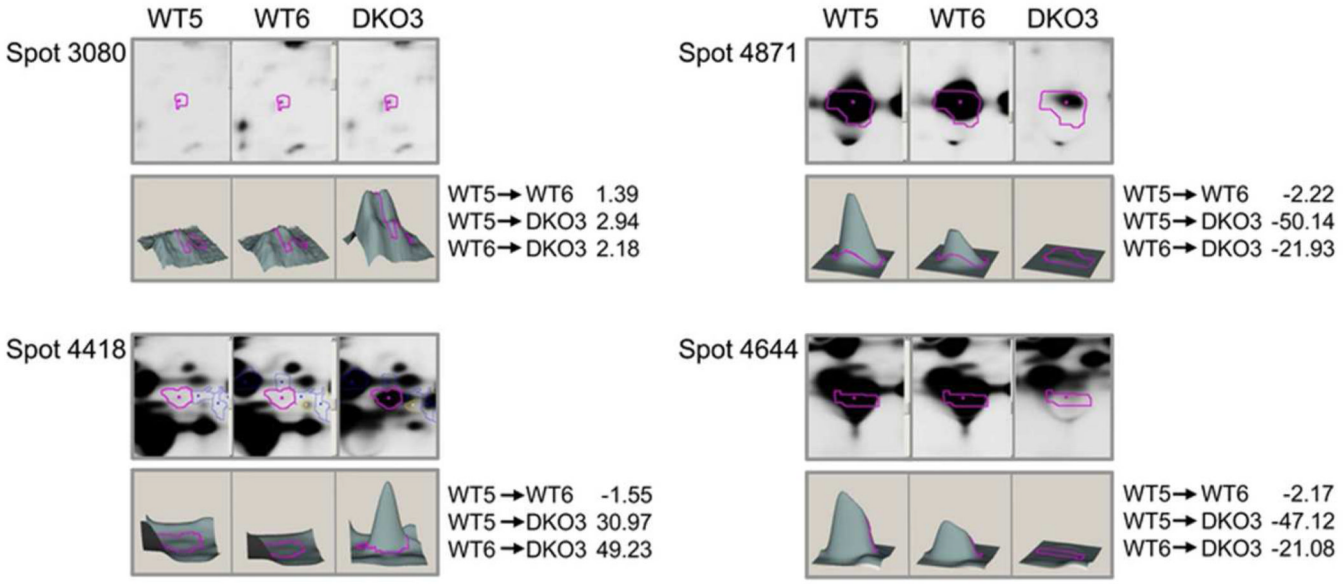

Figure 4.

(A) Changes in abundances in lens protein spots in lens epithelial fractions of WT and DKO lenses by mass spectrometry. Differentially expressed protein spots from the 2D-DIGE gel shown in Figure 2 were picked and analyzed. The 3D data sets for representative proteins in two WT (WT5 and WT6) and the DKO3 sample are shown. Fold changes between each sample are indicated on the right. See Table 2 for the identity of proteins present in each protein spot.

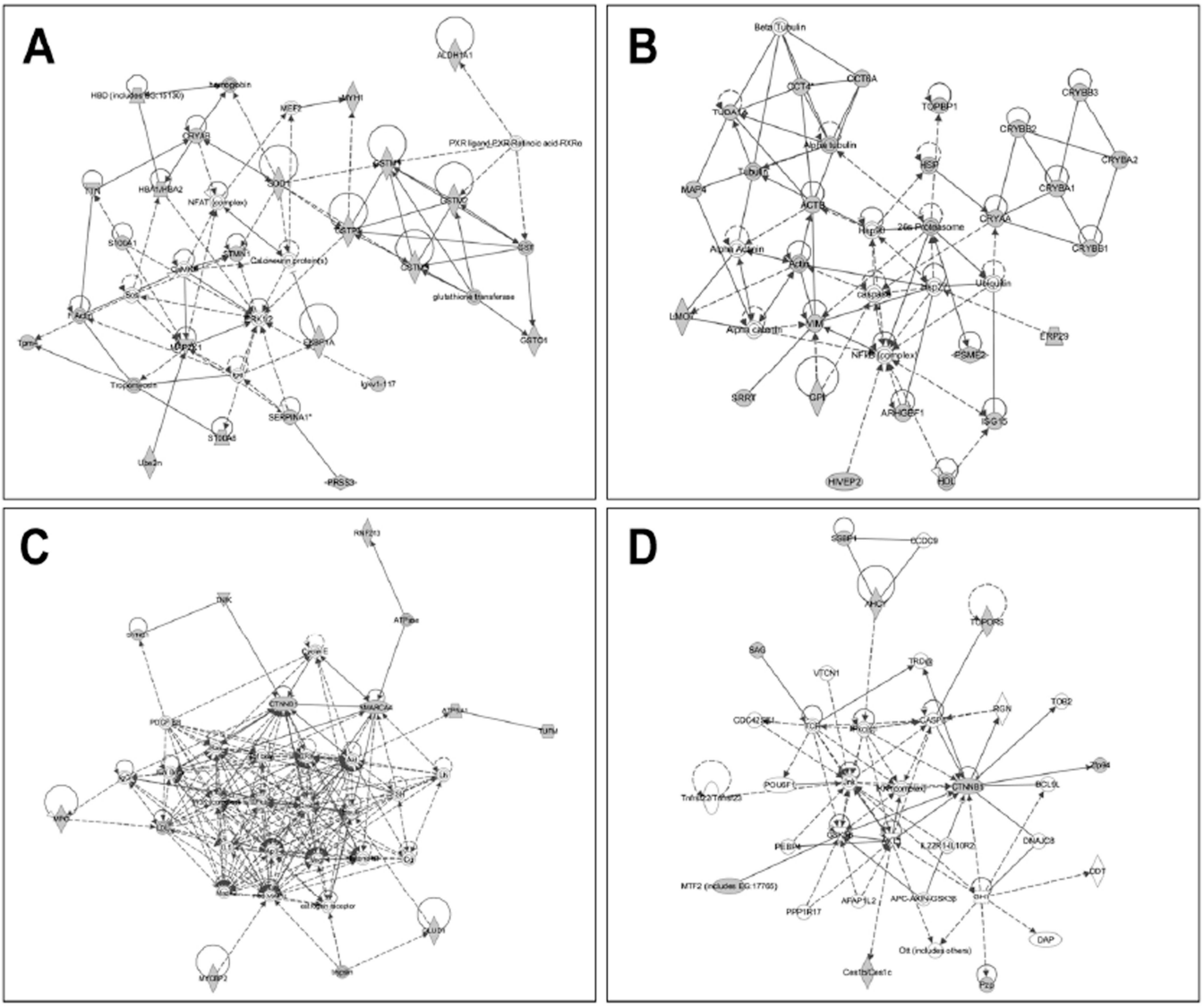

Figure 5.

Networks revealed by Ingenuity Pathway Analysis (IPA) of proteins that changed in amount in WT vs. DKO lenses. Four of the biological networks and pathways generated from input data (Tables 1–3) are shown. (A) A network with STMN and SOD1 at the hub. (B) A second network with heat shock proteins and cytoskeletal proteins at the hub. (C) A third network highlights CTNNB1 (β1-catenin) at the hub of the protein connectivity map. (D) Another network with CTNNB1 at its hub shows its interactions with caspase 8, RGN, and Zfp94 proteins. Proteins identified in Tables 1–3 within these pathways are shown in gray. Proteins with white background are molecules predicted by IPA. Lines indicate interaction, with arrowheads representing directionality. Absence of arrowheads refers to a binding interaction. Dotted lines represent an inferred or indirect interaction. An additional three networks are shown in Supplemental Figure S4.

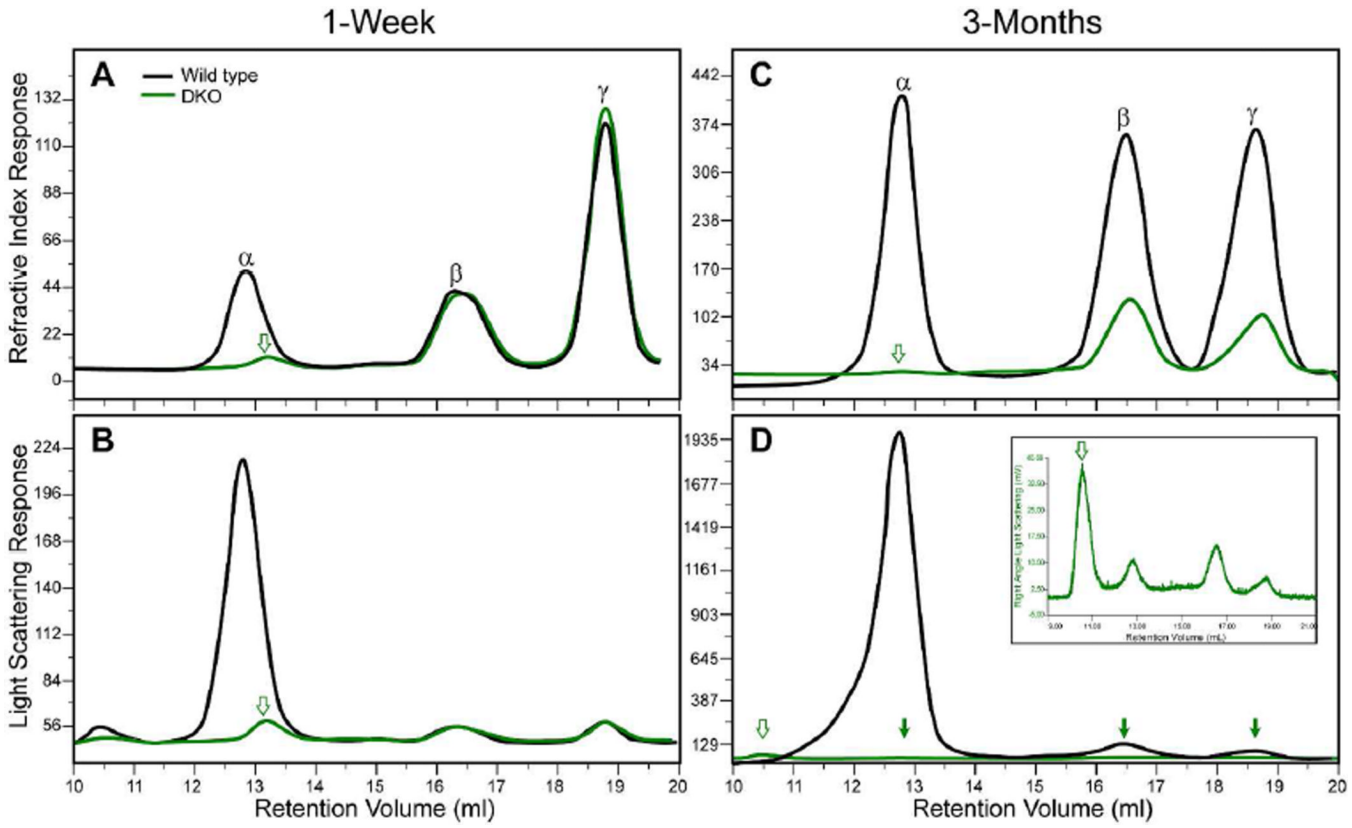

Figure 6.

GPC analysis of water-soluble proteins isolated from WT and DKO lenses. (A) RI profiles for postnatal WT and DKO lens proteins. (B) Light scattering profiles for 7-day-old WT and 9-day-old DKO lens proteins. (C) RI profiles for adult WT and DKO lens proteins. (D) Light scattering profiles for adult WT and DKO lens proteins. Open arrows in (A–D) indicate a discrete new band in DKO lenses that was not detected in WT lenses. The filled arrows in (D) indicate the position of small discrete bands in the light scattering profile of adult DKO lenses. The inset in (D) shows these DKO bands at a higher magnification.

Table 1

Mascot search results for mouse lens proteins of WT (WT1, WT2, WT3, WT4) and DKO (DKO1 and DKO2) 2-day-old lenses

Spot #	Protein ID	Accession #UNIPROT	# of assigned spectra	MW (kDa)	Fold change		
					WT1 vs. WT2	WT1 vs. DKO1	WT2 vs. DKO1
2744	Titin	A2ASS6	2	3906	1.02	−3.12	−3.21
2844	EH domain-containing protein 1,	Q9WVK	14	61	1.03	−3.41	−3.54
	T-complex protein 1 subunit zeta,	P80317	11	58			
	Bifunctional coenzyme A synthetase	Q9DBL7	2	62			
3027	βB1-crystallin	Q9WVJ5	3	28	−1.18	4.92	5.77
3037	Glucose-6-phosphate isomerase,	P06745	5	63	−1.00	−4.2	−4.23
	ATP synthase subunit alpha, mitochondrial,	Q03265	4	60			
	Retinal dehydrogenase 1,	P24549	4	54			
	T-complex protein 1 subunit delta,	Q3UJZ8	2	58			
	Polypyrimidine tract-binding protein 2	Q91Z31	2	57			
3194	Putative uncharacterized protein,	Q8C8Y8	3	38	−1.12	2.45	2.72
	Dynein, axonemal, heavy chain 9	B1AR51	2	512			
3669	cryaa protein,	Q569M7	12	20	−1.12	−5.97	−5.37
	Serine/threonine-protein kinase MRCK beta	Q7TT50	2	195			
3853	cryaa protein,	Q569M7	17	20	−1.00	−68.37	−68.7
	uncharacterized protein	D3Z0E6	5	27			
4946	cryaa protein,	Q569M7	10	20	1.07	−2.86	−3.08
	βB1-crystallin,	Q9WVJ5	4	28			
	ubiquitin-40S ribosomal protein S	P62983	4	18			
5251	βB2,	P62696	17	23	1.06	−8.58	−9.19

Spot #	Protein ID	Accession #UNIPROT	# of assigned spectra	MW (kDa)	Fold change		
					WT1 vs. WT2	WT1 vs. DKO1	WT2 vs. DKO1
	cryaa,	Q569M7	13	20			
	βA3/A1,	Q9QXC6	10	25			
	glutathione-S-transferase μ7,	Q80W21	6	26			
	βA2-crystallin,	Q9JJV1	5	22			
	glutathione-S-transferase μ5,	P48774	4	27			
	glutathione-S-transferase P1	P19157	2	24			
5258	cryaa,	Q569M7	22	20	1.05	−38.66	−40.87
	βA3/A1-crystallin,	Q9QXC6	7	25			
	MCG140784	Q792Z1	2	26			
5382	αB-crystallin,	P23927	32	20	1.32	−13.32	−17.7
	γS-crystallin,	O35486	10	21			
	cryaa,	Q569M7	7	20			
	γE-crystallin,	Q03740	6	21			
	βA2-crystallin	Q9JJV1	4	22			
5619	cryaa,	Q569M7	6	20	1.15	−4.39	−5.06
	βA3/A1-crystallin,	Q9QXC6	5	25			
	γE-crystallin,	Q03740	3	21			
	βA2-crystallin,	Q9JJV1	2	22			
	Gamma-crystallin B	P04344	2	21			
5626	cryaa,	Q569M7	11	20	1.12	−107.71	−121.84
	calcium-regulated heat stable protein,	Q9CR86	4	16			
	βA2-crystallin,	Q9JJV1	4	22			
	βA3/A1-crystallin	Q9QXC6	4	25			
5695	cryaa,	Q569M7	9	20	1.03	−82.51	−85.33
	γE-crystallin	Q03740	3	21			

Spot #	Protein ID	Accession #UNIPROT	# of assigned spectra	MW (kDa)	Fold change		
					WT1 vs. WT2	WT1 vs. DKO1	WT2 vs. DKO1
5783	cryaa,	Q569M7	10	20	−1.08	−13.33	−12.4
	βA3/A1-crystallin,	Q9QXC6	6	25			
	MCG140784,	Q792Z1	2	26			
	γE-crystallin,	Q03740	2	22			
	βA2-crystallin,	Q9JJV1	2	21			
6098	cryaa,	Q569M7	8	20	1.02	−2.8	−2.88
	catenin β-1,	Q02248	6	85			
	Testis-specific gene 10 protein,	Q6NY15	5	81			
	MCG124046,	Q9Z1R9	3	26			
	Alpha-2-macroglobulin	Q61838	3	166			
	Glutamate dehydrogenase 1, mitochondrial,	P26443	3	61			
	Uncharacterized protein,	D3YXG3	3	14			
	Alpha-1-antitrypsin 1–4,	Q00897	2	46			
	Metal-response element-binding transcription factor 2,	Q02395	2	67			
	Superoxide dismutase [Cu-Zn]	P08228	2	16			
6171	catenin β-1,	Q02248	8	85	−1.12	3.27	3.65
	MCG140784,	Q792Z1	4	26			
	Uncharacterized protein,	E9Q555	4	584			
	α-1-antitrypsin 1–4,	Q00897	3	46			
	Nesprin-1,	Q6ZWR6	3	1010			
	Liver carboxylesterase N,	P23953	3	61			
	Alpha-2-macroglobulin,	Q61838	2	166			
	Glutamate dehydrogenase 1, mitochondrial	P26443	2	61			
6278	Histone H2B (fragment),	A0JLV3	8	14	1.28	2.7	2.1
	catenin β-1,	Q02248	4	85			

Spot #	Protein ID	Accession #UNIPROT	# of assigned spectra	MW (kDa)	Fold change		
					WT1 vs. WT2	WT1 vs. DKO1	WT2 vs. DKO1
	Serine/threonine-protein kinase MRCK beta,	Q7TT50	3	195			
	Histone H2A type 1,	P22752	3	14			
	α-1-antitrypsin 1–4,	Q00897	2	46			
	Liver carboxylesterase N,	P23953	2	61			
	Histone H4,	P62806	2	11			
	Uncharacterized protein,	P23953	2	286			
	Alpha-1-antitrypsin 1–2	P22599	2	46			
6308	catenin β-1,	Q02248	8	85	1.22	2.37	1.93
	Histone H2B (fragment),	A0JLV3	5	14			
	Histone H2A type 1,	P22752	5	14			
	MCG140784,	Q792Z1	4	26			
	Rho guanine nucleotide exchange factor 1,	Q61210	3	103			
	Serine/threonine-protein kinase MRCK beta,	Q7TT50	2	195			
	60S ribosomal protein L23	P62830	2	15			
6404	catenin β-1,	Q02248	7	85	1.08	−1.14	−1.24
	cryaa,	M569M7	6	20			
	α-1-antitrypsin 1–4,	Q00897	3	46			
	Dynein, axonemal, heavy chain 9,	B1AR51	3	512			
	Alpha-2-macroglobulin	Q61838	2	166			
6463	Histone H2A type 1,	P22752	11	14	1.36	3.1	2.27
	catenin β-1,	Q02248	4	85			
	Histone H2B (fragment),	A0JLV3	4	14			
	Histone H4,	P62806	4	11			
	α-1-antitrypsin 1–4,	Q00897	2	46			
	Glutamate dehydrogenase 1, mitochondrial,	P26443	2	61			
	Transcription activator BRG1	Q3TKT4	2	181			

Spot #	Protein ID	Accession #UNIPROT	# of assigned spectra	MW (kDa)	Fold change		
					WT1 vs. WT2	WT1 vs. DKO1	WT2 vs. DKO1
6502	catenin β-1,	Q02248	6	85	1.36	2.81	2.06
	Histone H2A type 1,	P22752	5	14			
	MCG140784,	Q792Z1	5	26			
	Titin,	A2ASS6	5	3906			
	Histone H4,	P62806	4	11			
	Alpha-2-macroglobulin,	Q61838	4	166			
	LIM domain only 7,	A0T1J8	4	193			
	Microtubule-associated protein 4 (fragment),	Q60638	4	115			
	Hemoglobin subunit α,	P01942	3	15			
	Single-stranded DNA-binding protein, mitochondrial,	Q9CYR0	3	17			
	Histone H2B (fragment),	A0JLV3	2	14			
	Protein FAM5C	Q499E0	2	88			
6696	Putative uncharacterized protein,	Q8C2C1	44	20	1.44	3.3	2.28
	Histone H4,	P62806	19	11			
	Hemoglobin subunit alpha,	P01942	11	15			
	catenin β-1,	Q02248	7	85			
	Hemoglobin subunit 1β-2,	P02089	7	16			
	MCG140784,	Q792Z1	3	26			
	Alpha-1-antitrypsin 1–4,	Q00897	3	46			
	Alpha-crystallin B chain,	P23927	3	20			
	DNA topoisomerase 2-binding protein 1,	Q6ZQF0	3	169			
	Uncharacterized protein,	D3YZ11	3	93			
	Liver carboxylesterase N,	P23953	2	61			
	Zinc finger protein 292	Q9Z2U2	2	301			
7235	catenin β-1,	Q02248	6	85	1.18	2.26	1.9
	Protein SON,	Q9QX47	5	261			

Spot #	Protein ID	Accession #UNIPROT	# of assigned spectra	MW (kDa)	Fold change		
					WT1 vs. WT2	WT1 vs. DKO1	WT2 vs. DKO1
	MCG140784,	Q792Z1	4	26			
	Transcription factor HIVEP2,	Q3UHF7	4	267			
	Myeloperoxidase,	P11247	3	81			
	Alpha-2-macroglobulin,	Q61838	2	166			
	Uncharacterized protein,	E9Q6Y4	2	56			
	Protein S100-A6	P14069	2	10			
1093	Spectrin α2,	A3KG45	29	283	1.65	4.52	2.6
	Titin,	A2ASS6	5	3906			
	Catenin β1,	Q02248	4	85			
	serrate RNA effector molecule homolog,	Q99MR6	4	100			
	Phosphoribosylformylglycinamid ine synthase,	Q5SUR0	4	145			
	Alpha-2-macroglobulin,	Q61838	3	166			
	Ig heavy chain V region MOPC 47A,	P01786	2	13			
	Ig kappa chain V-II region 26-10	P01631	2	12			
3346	Actin cytoplasmic 1,	P60710	10	42	−1.19	−2.78	−2.45
	Catenin β1,	Q02248	7	85			
	Cryaa,	Q569M7	5	20			
	βA3/A1-crystallin,	Q9QX6	5	25			
	Titin,	A2ASS6	4	3906			
	MCG140784	Q792Z1	4	26			
	MCG124046	Q9Z1R9	4	48			
	Adenosylhomocysteinase	P50247	3	43			
	Dual specificity mitogen-activated protein kinase kinase 1	P31938	3	155			
	Tnik protein	B2RY17	2	26			
5697	Cryaa,	Q569M7	56	20	−1.25	−3.33	−2.8

Biochemistry. Author manuscript; available in PMC 2014 April 30.

Spot #	Protein ID	Accession #UNIPROT	# of assigned spectra	MW (kDa)	Fold change		
					WT1 vs. WT2	WT1 vs. DKO1	WT2 vs. DKO1
	Stathmin,	P54227	12	17			
	Catenin,	Q02248	4	85			
	Titin,	A2ASS6	4	3906			
	MCG140784,	Q792Z1|	4	26			
	γE-crystallin,	Q03740	4	21			
	Alpha-2-macroglobulin,	Q61838	3	166			
	Ig heavy chain V region MOPC 47A,	P01786	3	13			
	βA3/A1-crystallin,	Q9QXC6	2	25			
	Glutamate dehydrogenase 1, mitochondrial,	P26443	2	61			
	Gamma-crystallin B	P04344	2	21			
5902	Cryaa,	Q569M7	5	20	−1.04	−2.62	−2.65
	Titin,	A2ASS6	5	3906			
	Ig heavy chain V region MOPC 47A,	P01786	4	13			
	Catenin β1,	Q02248	3	85			
	Dynein heavy chain 5, axonemal,	Q8VHE6	3	528			
	Ubiquitin-conjugating enzyme E2 N	P61089	2	17			
6908	Cryaa protein,	Q569M7	5	20	1.37	2.8	1.94
	Catenin β1,	Q02248	5	85			
	MCG140784,	Q792Z1	4	26			
	Alpha-2-macroglobulin,	Q61838	4	166			
	Protein IWS1 homolog,	Q8C1D8	4	85			
	E3 ubiquitin-protein ligase Topors,	Q80Z37	4	117			
	Titin,	A2ASS6	3	3906			
	α-1-antitrypsin 1–4,	Q00897	3	46			
	Myosin-1,	Q5SX40	2	223			
	Probable E3 ubiquitin-protein ligase MYCBP2	Q7TPH6	2	518			

DKO1 proteins were labeled with Cy2, WT1 proteins labeled with Cy3, and WT2 proteins labeled with Cy5, then separated and analyzed on a single gel. As shown in the last six rows of the Table, an independent set of lens samples was analyzed by labeling WT3 proteins with Cy2, WT4 proteins with Cy3, and DKO2 proteins with Cy5.

Table 2

Mascot search results for mouse lens proteins of WT (WT5, WT6) and DKO3 lens epithelial fractions

Spot #	Protein ID	Accession # UNIPROT (gi)	# of assigned spectra	MW (kDa)	Fold change		
					WT5 vs. WT6	WT5 vs. DKO3	WT6 vs. DKO3
2787	vimentin,	P20152	14	54	1.21	3.3	2.81
	glucose-6-phosphate	P06745	7	63			
	isomerase,	P14168		58			
	pyruvate kinase isozymes M1/M2	P20152	2				
2799	vimentin,	P20152	55	54	−1.58	1.47	2.39
	tubulin alpha-1A chain	P68369	8	50			
3080	vimentin	P20152	28	54	1.39	2.94	2.18
3259	vimentin,	P20152	8	54	−2.49	−6.7	−2.62
	cryaa protein,	Q569M7	4	20			
	βA3/A1-crystallin,	Q9QXC6	3	25			
	Elongation factor Tu, mitochondrial,	Q8BFR5	3	50			
	βB2-crystallin	P62696	2	23			
3430	cryaa protein,	Q569M7	9	20	−3.07	−17.67	−5.59
	Quinone oxidoreductase-like protein 1	Q921W4	2	9			
4073	14-3-3 protein epsilon,	P63359	25	29	−1.04	−1.41	−1.32
	tropomyosin alpha-4 chain,	Q6IRU2	5	28			
	cryaa protein	Q569M7	4	20			
4104	βB1-crystallin,	Q9WVJ5	34	28	−1.39	−2.6	−1.82
	S-methyl-5’ thioadenosine phosphorylase,	Q9CQ65	5	31			
	glutathione S-transferase omega	O09131	2				
4115	proteasome activator complex subunit 2,	P97372	6	27 20	1.02	3.75	3.78

Spot #	Protein ID	Accession # UNIPROT (gi)	# of assigned spectra	MW (kDa)	Fold change		
					WT5 vs. WT6	WT5 vs. DKO3	WT6 vs. DKO3
	alpha-crystallin B chain,	P23927	3	20			
	Cryaa protein	Q569M7	2				
4175	endoplasmic reticulum resident protein 29,	P57759	10	29	1.72	−2.57	−4.31
	βB1-crystallin	Q9WVJJ					
4224	endoplasmic reticulum resident protein 29,	P57759	9	29	2.24	2.48	1.14
	Alpha-crystallin B chain,	P23927	3	20			
	MCG140784	Q792Z1	2	26			
4418	βB2-crystallin	P62696	12	23	−1.55	30.97	49.23
4421	βB3-crystallin,	Q9JJU9	18	24	−1.5	7.19	11.11
	βB2-crystallin,	P62696	14	23			
	glutathione S-transferase	P15626	13	26			
	Mu2,		2	20			
	alpha-crystallin B chain	P23927					
4425	βB2-crystallin	P62696	21	23	−3.58	−1.64	2.24
4430	βB2-crystallin	P62696	14	23	−1.38	7.4	10.52
4431	βB2-crystallin	P62696	5	23	−1.53	3.57	5.61
4443	βB2-crystallin,	P62696	5	23	−2.46	16.71	42.34
4446	βB2-crystallin	P62696	4	23	−1.01	5.62	5.81
4457	βB3-crystallin,	Q9JJU9	9	24	−2.24	−3.69	−1.6
	βB2-crystallin,	P62696	7	23			
	alpha-crystallin B chain	P239927	6	20			
4491	βB2-crystallin	P62696	2	23	−1.09	2.53	2.83

Spot #	Protein ID	Accession # UNIPROT (gi)	# of assigned spectra	MW (kDa)	Fold change		
					WT5 vs. WT6	WT5 vs. DKO3	WT6 vs. DKO3
4636	βB2-crystallin	P62696	2	23	−1.16	3.74	4.47
5247	alpha-crystallin B chain,	P23297	2	20	−1.27	3.27	4.26
	ubiquitin-like protein ISG15	Q64339	2	18			

WT5 proteins were labeled with Cy2, WT6 proteins were labeled with Cy3, and DKO3 proteins were labeled with Cy5, then analyzed on a single gel.

Table 3

Mascot search results for mouse lens proteins of WT (WT5, WT6) and DKO3 lens epithelial fractions to confirm protein deletion

Spot #	Protein ID	Accession # UNIPROT	# of assigned spectra	MW (kDa)	Fold change		
					WT5 vs. WT6	WT5 vs. DKO3	WT6 vs. DKO3
2789	Glucose-6-phosphate	P06745	15	63	1.32	−4.81	−6.16
	isomerase,	P24549	3	54			
	Retinal dehydrogenase 1,	Q03265	2	60			
	ATP synthase subunit α mitochondrial,	P80315	2	58			
	T-complex protein 1 subunit delta						
3430	cryaa protein,	Q569M7	12	20	−3.07	−17.67	−5.59
	3’(2’),5’biphosphate nucleotidase 1	Q9Z0S1	8	33			
4175	endoplasmic reticulum resident protein 29,	P57759	11	29	1.72	−2.57	−4.31
	cryaa protein	Q569M7	4	20			
4474	cryaa protein,	Q569M7	19	20	−2.25	−27.82	−12.04
	β-A3/A1 crystallin,	Q9QXC6	7	25			
	βB2-crystallin,	P62696	5	23			
	βS-crystallin,	O35486	4	21			
	βA2-crystallin	Q9JJV1	3	22			
4485	βB2-crystallin,	P62696	42	23	−3.52	−7.04	−1.94
	cryaa protein	Q569M7	3	20			
4644	alpha-crystallin B chain,	P23927	22	20	−2.17	−47.12	−21.08
	γS-crystallin,	O35486	21	21			
	βB2-crystallin	P62696	4	23			
4778	cryaa protein,	Q569M7	2	20	−3.4	−45.61	−13.04
	alpha-rystallin B	P23297	2	20			
	chain,	Q64339		18			

Spot #	Protein ID	Accession # UNIPROT	# of assigned spectra	MW (kDa)	Fold change		
					WT5 vs. WT6	WT5 vs. DKO3	WT6 vs. DKO3
	calcium-regulated heat stable protein		2				
4793	alpha-crystallin B chain,	P23927	16	20	−2.38	−9.4	−3.83
	γS-crystallin,	O35486	4	21			
	γE-crystallin	Q03740	3	21			
4871	cryaa protein	Q569M7	51	20	−2.22	−50.14	−21.93
5020	cryaa protein	Q569M7	185	20	−4.82	−35.85	−7.22
5532	alpha-crystallin B chain,	P23927	9	20	−1.82	−6.84	−3.65
	cryaa protein,	Q569M7	7	20			
	histone H4,	P62805	4	11			
	hemoglobin subunit α,	P01942	3	12			
	peptidyl-propyl cis-trans isomerase FKBP1A,	P26883	3	15			
	βB2-crystallin	P62696	2	23			

WT5 proteins were labeled with Cy2, WT6 proteins were labeled with Cy3, and DKO3 proteins were labeled with Cy5, then analyzed on a single gel.

Table 4

Molecular weight (M_w) and R_h of crystallins in WT and DKO mice

Age (days)	Genotype	M_w (kDa)	R_h (nm)	M_w (kDa)	R_h (nm)	M_w (kDa)	R_h (nm)	M_w (kDa)	R_h(nm)
		α-Crystallin		**Additional peak or shoulder**		**β-Crystallin**		**γ-Crystallin**	
7	WT	682.082	8.140	n.d	n.d	43.690	3.283	19.295	2.278
117	WT	1141	9.818	n.d	n.d	54.647	3.195	23.988	2.290
9	DKO	n.d	n.d	327.946 (small peak near α)	**	52.034	3.244	23.780	2.466
107	DKO	n.d	n.d	297.690 (shoulder before β)	5.141	70.677	3.371	26.737	2.731

Proteins from an adult DKO lenses were largely water-insoluble. Due to insufficient soluble protein, the R_h values from viscosity measurements for the DKO lenses were used. The DKO lens proteins exhibited a shoulder before the main β-crystallin peak (Figure 4C and D). An additional peak with an estimated molecular weight of > 10×10^6 was observed in 9-day-old DKO lenses (Figure 4B).

R_h, hydrodynamic radius; n.d, not detected.

** R_h was approximated.